



OPEN

Enhanced tetracycline degradation with TiO₂/natural pyrite S-scheme photocatalyst

Masoumeh Hasham Firooz¹, Azra Naderi^{2,3}, Masoud Moradi⁴ & Roshanak Rezaei Kalantary^{2,3}✉

In this study, TiO₂ nanoparticles were employed as a photocatalyst for the degradation of tetracycline (TC) under visible light irradiation. The TiO₂ nanoparticles were decorated on natural pyrite (TiO₂/NP) and characterized using XRD, FTIR, and SEM–EDX methods. This study evaluated the impacts of various operational parameters such as pH, catalyst dosage, initial TC concentration, and light intensity on TC removal. The findings revealed that under optimal conditions (pH 7, catalyst: 2 g/L, TC: 30 mg/L, and light intensity: 60 mW/cm²), 100% of TC and 84% of TOC were removed within 180 min. The kinetics of TC elimination followed a first-order model. The dominant oxidation species involved in the photocatalytic elimination of TC was found to be ·OH radicals in the TiO₂/NP system. The reuse experiments showed the high capability of the catalyst after four consecutive cycles. This study confirmed that the TiO₂/NP system has high performance in photocatalytic TC removal under optimized experimental conditions.

Keywords Photocatalytic removal, TiO₂/NP, TiO₂, Pyrite, Tetracycline (TC), Pharmaceutical wastewater

Pharmaceutical compounds (PCs) are known to be potential contaminants of water resources due to their extensive use in medical purposes, which results in the release of high concentrations of these compounds into pharmaceutical and hospital wastewater¹.

Numerous studies have been interested in the occurrence of pharmaceutical compounds as emerging pollutants in water resources owing to the threats these compounds at low concentrations pose to the ecosystem, human health, and water resource quality^{2,3}.

Antibiotics are one of the pharmaceutical compounds categories which are discharged into water matrices from pharmaceutical factories, hospitals, municipal sewages, and livestock farms⁴. There may be major environmental problems due to the rising production and excessive usage of these substances, which may be hazardous to both humans and animals^{5,6}. The majority of them are non-biodegradable, which means that they can remain in the ecosystem for extensive periods of time and generate antibiotic resistance bacteria⁷. Among these compounds, tetracycline (TC) has been found in wastewater effluent and in trace amounts in surface water^{8–11}. Since TC is resistant to microbial degradation, biological wastewater treatment will not be able to complete the removal of this pollutant, and it can be considered a challenge for wastewater treatment systems¹². As a result, because of its adverse impacts, the development of sustainable technologies is essential to eliminate this pollutant from environmental aqueous.

TC has been eliminated from liquid solutions using a variety of methods, including biological, chemical, and physical processes^{11,13–15}. However, most of these processes are expensive or unsuitable for effectively removing TC. Because of its high success in eliminating refractory organic pollutants from wastewater, advanced oxidation processes (AOPs) have gained significant attention in recent years^{16,17}. Among these methods, photocatalytic oxidation stands out as a particularly intriguing choice for reducing contaminants. The basis of this process is the employment of semiconductors in the presence of light, and it is highly effective, straightforward, fast, and has minimal toxicity^{18–21}. The photocatalytic features of various semiconductors in the elimination of various antibiotics are presented in Table 1.

¹Department of Environmental Health Engineering, School of Public Health, Tehran University of Medical Sciences, Tehran, Iran. ²Department of Environmental Health Engineering, School of Public Health, Iran University of Medical Sciences, Tehran, Iran. ³Research Center for Environmental Health Technology (RCEHT), Iran University of Medical Sciences, Tehran, Iran. ⁴Research Center for Environmental Health Determinants of Health (RCEHD), Health Institute, Kermanshah University of Medical Sciences, Kermanshah, Iran. ✉email: rezaei.r@iums.ac.ir

No	Catalyst	Light source	Experimental conditions	Antibiotic	Efficiency (%)	Ref
1	CZ@T-GCN	Simulated sunlight (250 W xenon)	[C ₀]: 60 mg/L, [catalyst]: 0.9 g/L, [pH]:7, [time]:120 min	Amoxicillin	100	4
2	Cu-TiO ₂ /GO	UV light (300 W mercury lamp)	[C ₀]: 20 mg/L, [catalyst]: 0.5 g/L, [pH]:7, [time]:90 min	Tetracycline hydrochloride	98	38
3	TiO ₂	Visible light	[C ₀]: 10 mg/L, [catalyst]:0.2 g/L, [temperature]:25 °C, [time]:120 min	Tetracycline	56.7	23
4	ZnO@BiOBr	Visible light	[C ₀]: 20 ppm, [catalyst]: 0.5 g/L, [pH]:6, [time]:112 min	Metronidazole	87.72	39
5	CdS/BiOBr	Visible light	[C ₀]: 10 mg/L, [catalyst]: 50 mg, [pH]:7, [time]:240 min	Norfloxacin	98.3	40
				ciprofloxacin	96.7	
6	Ti-MOF/Ag/NiFeLDH	Visible light (300 W xenon)	[C ₀]: 15 mg/L, [catalyst]: 10 mg, [time]:70 min	Levofloxacin	92	19
7	BiVO ₄	Sunlight	[C ₀]: 10 mg/L, [catalyst]: 50 mg, [time]:240 min	Oxytetracycline	83	41
		visible light			55.5	
8	Ag-ZnO	UV light	[C ₀]: 10 mg/L, [catalyst]: 50 mg, [time]:180 min	Ofloxacin	100	42
		Sunlight			100	
9	Zn _{1-x} Mg _x Fe ₂ O ₄	Visible light (300 W xenon)	[C ₀]: 10 mg/L, [catalyst]: 0.3 mg/ml, [temperature]:30 ± 0.5 °C, [pH]:7, [time]:90 min	Sulfadiazine	99.1	43
10	Urea/TiO ₂ /ZnFe ₂ O ₄ /zeolite	UV-visible light	[C ₀]: 100 mg/L, [catalyst]:2 g/L, [pH]:7, [time]:120 min	Cephalexin	74	44
			[C ₀]: 100 mg/L, [catalyst]:2 g/L, [pH]:5, [time]:120 min	Metronidazole	70	
11	Ta ₃ N ₅ /CdS	Visible light (300 W xenon)	[C ₀]: 20 mg/L, [catalyst]: 30 mg, [time]: 50 min	Tetracycline	90.5	45
12	MIL-101(Fe)/BiOBr	Visible light (300 W xenon)	[C ₀]: 10 mg/L, [catalyst]:25 mg, [pH]:6.8, [time]: 40 min	Enrofloxacin	84.4	46
13	MIL-101(Fe)/Bi ₂ WO ₆	Visible light	[C ₀]: 20 mg/L, [catalyst]:20 mg, [pH]: 5.2, [time]: 60 min	Tetracycline	82.8	47
14	ZnO/g-C ₃ N ₄	Visible light (fluorescent bulb)	[C ₀]: 1 mg/L, [catalyst]:0.05 g/L, [pH]: 8, [time]: 120 min	Ciprofloxacin	93.8	48

Table 1. Different photocatalysts applied for antibiotic degradation.

Among them, titanium dioxide (TiO₂) is one of the greatest broadly used catalysts because of its outstanding performance, chemical resistance, availability, low toxicity, and inexpensive cost^{22,23}. Nevertheless, the inherent characteristics of pure TiO₂, namely its substantial band gap and swift recombination rate of electron-hole pairs generated, hinder proper photocatalyst efficiency under visible light^{19,22}. Additionally, in practical uses, since nanoparticles are applied as suspension, separating and recovering nanoparticles from treated aqueous solution is a serious problem²⁴. Therefore, the catalytic activity of TiO₂ can be increased through transition metals doping and substrates immobilizing approaches²⁵⁻²⁷. In other hands, one of the typical strategy for improving photocatalyst performance is to create heterogeneous catalysts that provide effective spatial separation of photocarriers. In particular, S-scheme photocatalysts with a strong internal electric field (IEF) demonstrate considerable advantages in photocarrier separation efficiency and photoreduction capabilities²⁸⁻³¹. These improved S-scheme catalysts still have issues such as easy compaction and difficult separation and recovery, which may lead to secondary contamination, limiting their industrial applicability^{32,33}.

Natural semiconductor minerals (NSMs) have been utilized to boost the photocatalytic efficacy when irritated by visible light due to their impurities and complex crystal imperfections. In addition, their low cost and availability can significantly reduce treatment costs³⁴. Natural pyrite (NP), also known as FeS₂, is a readily accessible non-semiconductor material (NSM) that possesses a reasonably high potential for optical absorption due to its modest band gap of 0.95 eV. This makes it a promising candidate for modifying TiO₂, offering a practical alternative³⁵. As a result, immobilizing nanoparticles on pyrite structures can be an excellent approach to stabilize nanoparticles and provide higher photocatalytic contact surface area, which promotes photocatalytic activity.

Recently, S-scheme heterojunction photocatalysts have attracted the attention of many researchers. In this approach, due to the heterojunction of the S-scheme, the separation rate of photogenerated electrons and holes improved, and at the same time, the redox potential does not decrease and conductivity is also preserved³⁶. In S-scheme photocatalysts, electrons move from the conduction band of one semiconductor to the valence band of the other semiconductor due to the internal electric field at the interface between the two semiconductors. This creates an S-shaped electron migration path. Therefore, electrons and holes that have a strong redox potential are preserved, and those with a weaker strong redox potential are transferred and consumed³⁷.

Given the foregoing, the principle aim of the current study is to assess the effectiveness of natural pyrite supported TiO₂ (TiO₂/NP) in TC elimination using the visible light. Additionally, the impact of various factors, including pH, catalyst quantity, initial TC concentration, light intensity, the existence of mineral ions on the photocatalytic removal of tetracycline, as well as mineralization degree by TiO₂/NP, was evaluated.

Materials and methods

Chemicals

The tetracycline powder, obtained from Sigma-Aldrich Co. (USA), with a purity of at least 88% and meeting HPLC grade standards, was used in the study. The chemical properties of tetracycline are detailed in Table 2. The pyrite mineral used in this study was obtained from the Department of Mine Engineering at Tehran University in Iran. All other chemicals, including tert-butyl alcohol (TBA), potassium iodide (KI), oxalic acid, nitric acid, ethanol, and tert-butyl titanate (TBT), were acquired from Merck Company (Germany) and utilized without any further purification. Deionized water (DIW) was utilized in the creation of the watery mixtures.

Synthesis of TiO₂/NP

The pyrite stone was machine-crushed and milled, then ultrasonicated for 5 min in ethanol (95%). After being washed in HNO₃ (1 M) to remove external contaminants, the resulting pyrite was rinsed multiple times in deionized water and dried at room temperature. All pyrite particles were sieved through 200 mesh (74 μm)^{35,49}. Afterward, the pyrite powder was mixed with a specific quantity of Ti(C₄H₉O)₄ dissolved in ethanol to synthesize TiO₂/NP. The resulting mixture was stirred with a magnetic stirrer for 2 h before being dried at 80 °C. Finally, The dried as-prepared was then heated to 550 °C for 2 h and cooled to room³⁵.

Characterization

XRD analyses were carried out to crystalline phase determination of synthesized catalysts. The surface morphology and chemical composition of pyrite, and the synthesized nanocomposite were determined by Scanning Electron Microscopy (SEM) equipped with energy-dispersive X-ray spectroscopy chemical analysis (EDS). Fourier transforms infrared spectroscopy (FTIR) was conducted in the range of 4,000 to 500 cm⁻¹ to determine functional groups on the surface of the catalyst. The diffuse reflectance spectroscopy (DRS) technique was used to analyze the optical properties of the samples. The details of XRD, FTIR, and SEM–EDX techniques were described in previous study³⁵.

Tetracycline degradation using photocatalytic approach

The elimination of TC was investigated using the photocatalytic approach in a 500 ml rectangular, black-colored, plexiglass reactor containing a 100 ml sample. Four LED lamps with a maximum wavelength of 450 nm and 15mW/cm² intensity were installed in the central upper part of the reactor. All experiments took place in a batch system. The photocatalytic potential of the nanocomposite was assessed by introducing a particular quantity of the catalyst into the solution. Later adjusting the pH value of the solution with hydrochloric acid and sodium hydroxide (0.01 M), the visible lamps were turned on and the samples were mixed at 200 rpm with a magnetic stirrer for the required time. Afterward, 1 ml of sample was extracted at predetermined intervals. The remaining level of the residual pollutant was measured by utilizing high-performance liquid chromatography (HPLC) with an Agilent 1200 Infinity Series instrument from the United States. The effect of varying process parameters including pH (3, 7, and 9), TiO₂/pyrite dosage (0.1, 0.5, 1, 2, and 3 g/L), initial tetracycline concentration (10, 20, 30, 40 and 50 mg/L), and the intensity of visible light (15, 30, and 60 mW/cm²) on TC removal were examined. Total organic carbon (TOC) analysis was conducted in order to determine the mineralization value during pollutant degradation by photocatalytic approach. Furthermore, tert-butanol (0.5 mmol/L), potassium iodide (0.5 mmol/L), and Cr (VI) (0.5 mmol/L) were employed to examine the impact of the reactive species generated throughout the photocatalytic reaction.

Results and discussion

Catalyst characterization

The details of XRD, FTIR, and SEM–EDX results were described in previous study³⁵. XRD patterns of natural pyrite (NP) and TiO₂/NP are shown in Fig. 1a and b. The findings demonstrated that following calcination during the TiO₂/NP synthesis process, the pyrite's XRD pattern had slightly altered. The intensity of the peak at 2θ = 73.13° decreased, while the peak at 2θ = 76.37° faded. The results also showed that pyrrhotite (Fe_(1-x)S) was allocated to the peak at 2θ = 30° (220)⁵⁰. The emergence of pyrrhotite could be attributed to the influence of the calcination procedure on the configuration of FeS₂⁵¹. Furthermore, XRD analysis has verified significantly intensified pyrite diffraction peaks within the TiO₂/NP sample. This observation suggests that there is a notable concentration of pyrite present in the TiO₂/NP^{35,52}.

Figure 2 depicts the FTIR distinctive peaks of TiO₂/NP. The details of FTIR spectra of pyrite and synthesized catalyst were presented in our previous study^{35,53}. FTIR spectra of TiO₂/NP indicate that the two peaks around

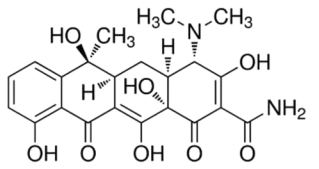
Chemical structure	Molecular formula	M _w (g/mol)	solubility	PK _{a1}	PK _{a2}	PK _{a3}
	C ₂₂ H ₂₄ N ₂ O ₈ ·xH ₂ O	444.43	1.7 g/L	3.30	7.68	9.69

Table 2. Characteristics of tetracycline powder.

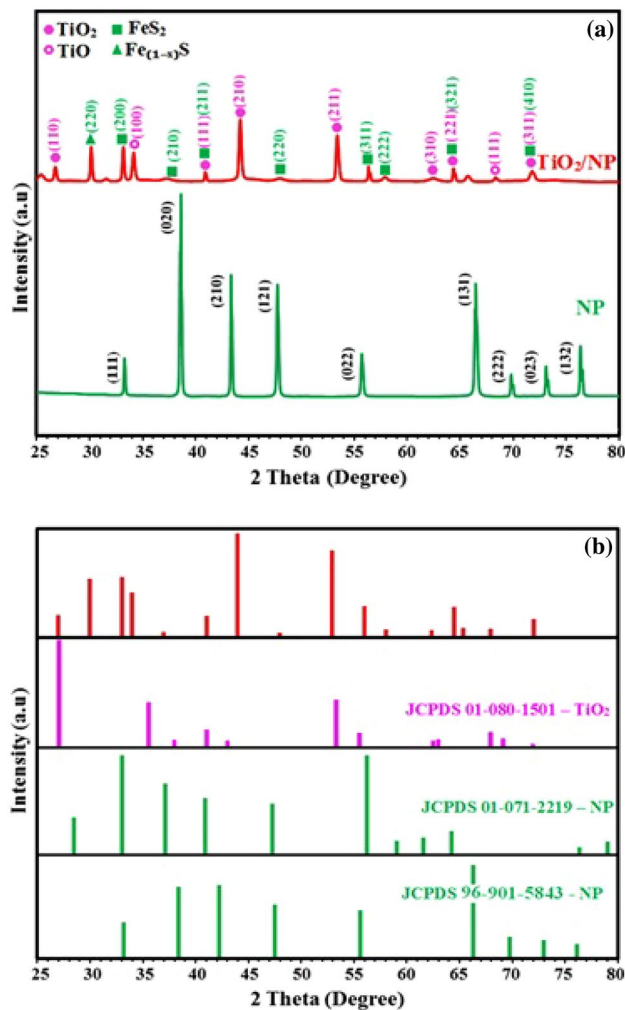


Figure 1. (a) and (b) XRD patterns of NP and TiO_2/NP .

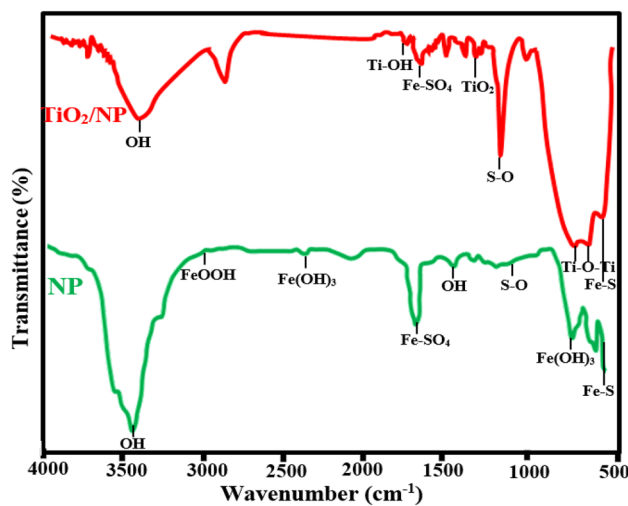


Figure 2. FTIR spectrum of NP and TiO_2/NP .

2360 and 2925 cm^{-1} observed in pyrite are attributed to iron (III) hydroxide and goethite, respectively; these peaks were diminished subsequent to the decoration of TiO_2 with pyrite. The findings suggest a decrease in the Fe_2O_3 coating on the NP⁵⁵. The emergence of the peak observed at 1630 cm^{-1} is ascribed to the Ti–OH functional group, which implies the existence of TiO_2 on the pyrite's surface⁵⁴.

The morphological characteristics of pyrite and TiO_2/NP are depicted in Fig. 3a,b. As illustrated in Fig. 3a, the natural massive structure and irregular exterior surface of the pyrite enhance its surface area. This exposes more of the iron present on the catalyst surface, facilitating a high quantity formation of ROS⁵⁵. EDS results (Fig. 3a) show that sulphur (S) and iron (Fe) are the predominant elements, while oxygen (O) and carbon (C) are present. The attendance of C and O could be assigned to the adsorption of organic substances or iron oxide during grinding and milling. SEM analysis (Fig. 3b) reveals that pyrite particles are composed of TiO_2 and exhibit agglomerated and irregular features. The successful immobilization of TiO_2 onto the pyrite surface leads to a lustrous color and reduced sharpness of pyrite edges. The synthesis of TiO_2/NP was confirmed by the detection of Ti, O, S, and Fe in the catalyst. Additionally, the weight percentage of oxygen increased after impregnation, indicating the presence of oxygen within the TiO_2 crystal structure⁵⁶.

The optical properties of NP and TiO_2/NP were analyzed using the DRS technique, as shown in Fig. 4a,b. The results revealed that the absorbance spectra of NP and TiO_2/NP were observed at 810 nm and 490 nm, respectively. These values correspond to the band gaps of NP and TiO_2/NP , which are determined to be 2.23 eV and 2.84 eV, respectively. The findings confirm that NP can reduce the band gap of TiO_2 , resulting in an increased generation of ROS when exposed to visible light irradiation.

Impact of varying reaction conditions on photocatalytic process

Influence of pH

The photocatalytic process is significantly influenced by pH due to several factors, including alterations in the catalyst surface charge, the degree of ionization, and the formation of diverse pollutant species at varying pH levels^{1,16}. Therefore, the impact of the initial pH on the photocatalytic elimination of TC was evaluated across three distinct pH levels, including acidic, neutral, and basic.

Figure 5a1, a2 demonstrate that the most significant removal of TC was observed at a neutral pH, with a corresponding $k_{\text{obs}} = 0.0165 \text{ min}^{-1}$. As mentioned, as well as alterations in the surface charge of catalyst, different forms of TC are generated as the pH values change^{6,57}. The photocatalyst demonstrates low TC adsorption at different pH levels, resulting in only 26.7%, 63.5%, and 48.1% of TC being adsorbed by TiO_2/NP at pH 3, 7, and 9 respectively. The adsorption process depends on the nature of the adsorbent and adsorbate. TC has three pK_a values: 3.3, 7.7, and 9.7, which can affect its hydrolysis and precipitation processes. At $3.3 < \text{pH} < 7.7$, the molecular structure of TC is TCH_3^+ ; at $7.7 < \text{pH} < 9.7$, it is TCH^0 and TCH^- ; and at $\text{pH} > 9.7$, it takes the TCH^{2-} form. Since the point of zero charge (pH_{pzc}) of $\text{TiO}_2/\text{pyrite}$ is 6.95 under acidic conditions ($\text{pH} < \text{pH}_{\text{pzc}}$), the composite had a positive surface charge, while, at acidic pH, TC existed in the positive form (TCH^{3+})⁵⁷. Consequently,

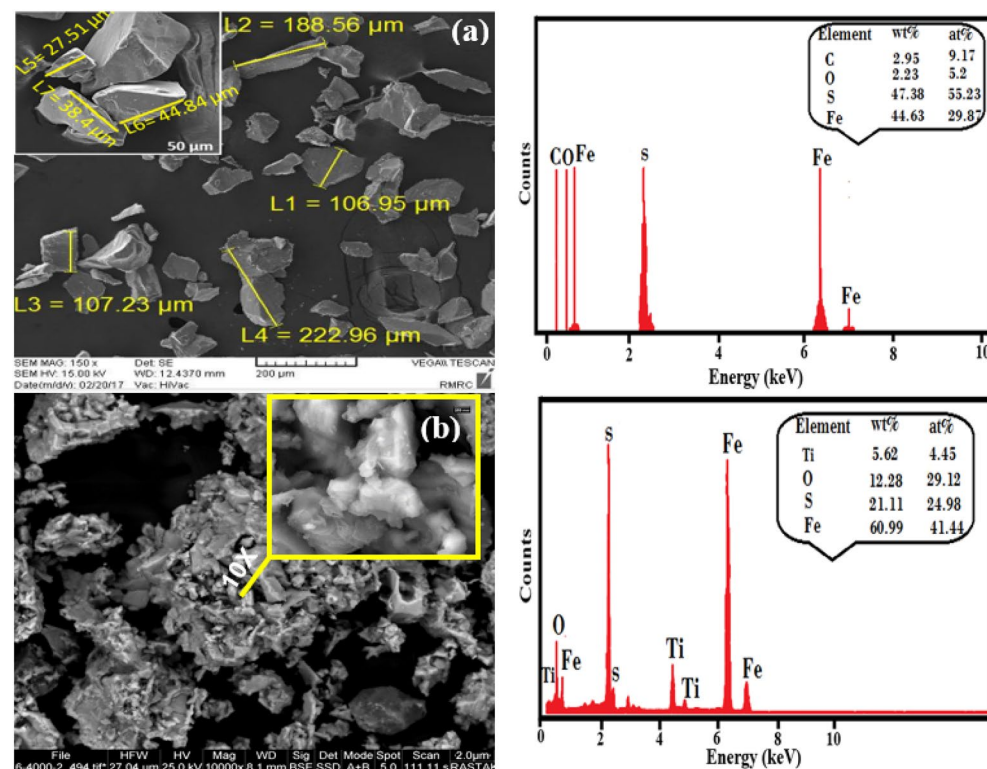


Figure 3. The image of SEM–EDS (a) NP and (b) TiO_2/NP .

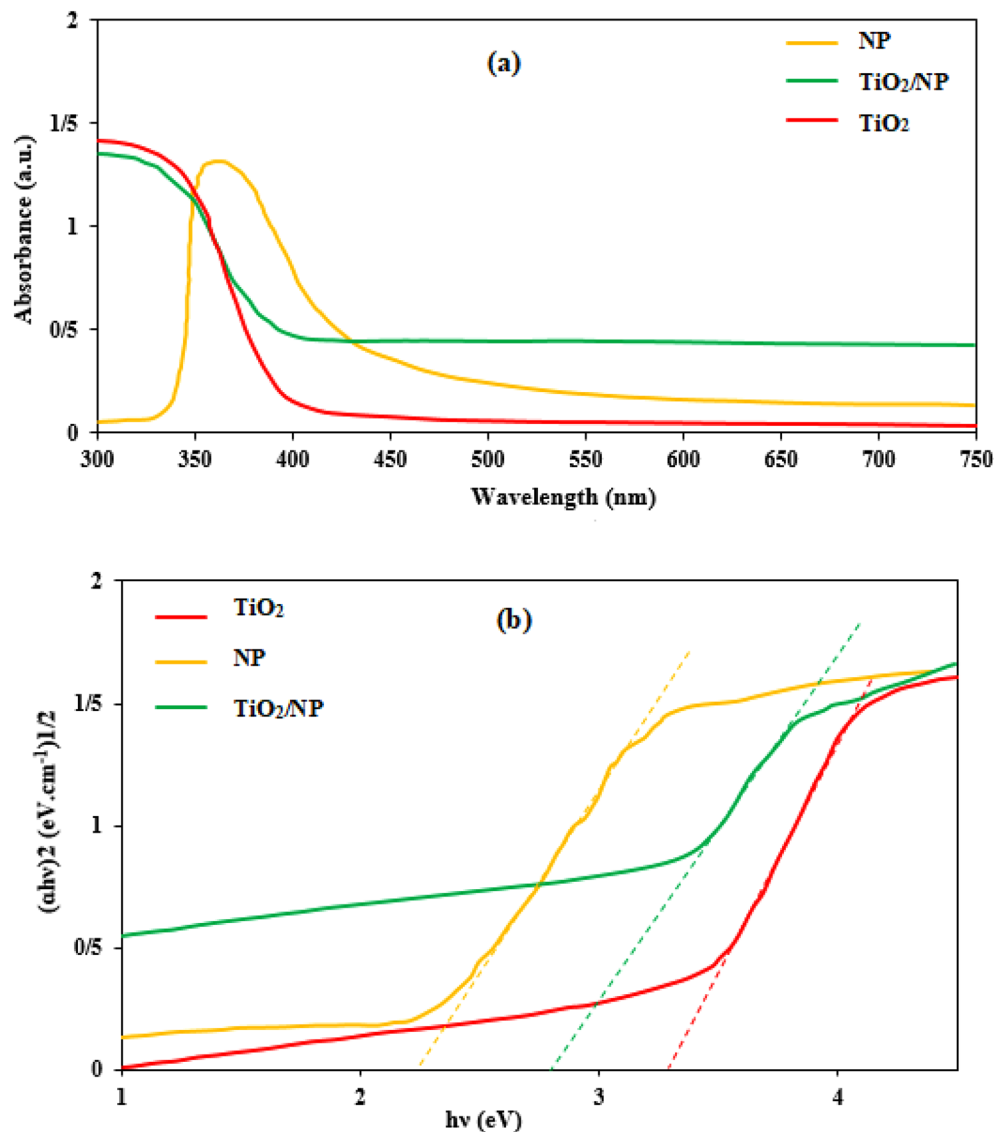


Figure 4. The DRS results of TiO₂, NP and TiO₂/NP.

the presence of a solid repulsive force between the positively charged ions and the charged surface of the TiO₂/NP hindered the adsorption process of ions on the surface of the catalyst. This resulted in a decrease in the TC removal under acidic pH conditions^{22,58}. The decline in photocatalytic efficacy at basic pH may be ascribed to the electrostatic repulsion between the negative surface charge of the catalyst (pH > pHPzc) and the negative ions of TC that are generated at higher pH levels^{59–61}. At a pH of 7, the concentrations of positive and negative charges are nearly balanced. However, due to the minimal presence of negative charge on the catalyst surface at pH 7, and the predominance of TC molecules in the TCH³⁺ form, maximum absorption has occurred. Moreover, in the photocatalytic process, surface hydroxyl radicals, in addition to bulk hydroxyl radicals, are generated, which decompose the absorbed molecules.

Although alkaline pH conditions generate a greater quantity of the ·OH, that can enhance the removal process as a reactive oxidative species (ROS), the photocatalytic efficiency is diminished as a consequence of the ferrous and ferric precipitation and the generation of Fe(OH)₂⁴⁺. This is attributed to its lower catalytic activity in comparison to Fe²⁺⁶². Conversely, the deposition and existence of these hydroxides at the catalyst surface hinder the photocatalytic elimination of TC⁶². Based on the findings, the neutral pH was elected as the optimum pH for further investigations.

Influence of TiO₂/NP concentration

The findings from investigating the impact of TiO₂/NP concentration on TC elimination (as depicted in Fig. 5b1) indicate that as the photocatalyst concentration raised from 0.1 to 2 g/L, the degradation efficacy of TC improved significantly, rising from 30.67% to 100% over a 180-min timeframe. According to the data presented in Fig. 5b2,

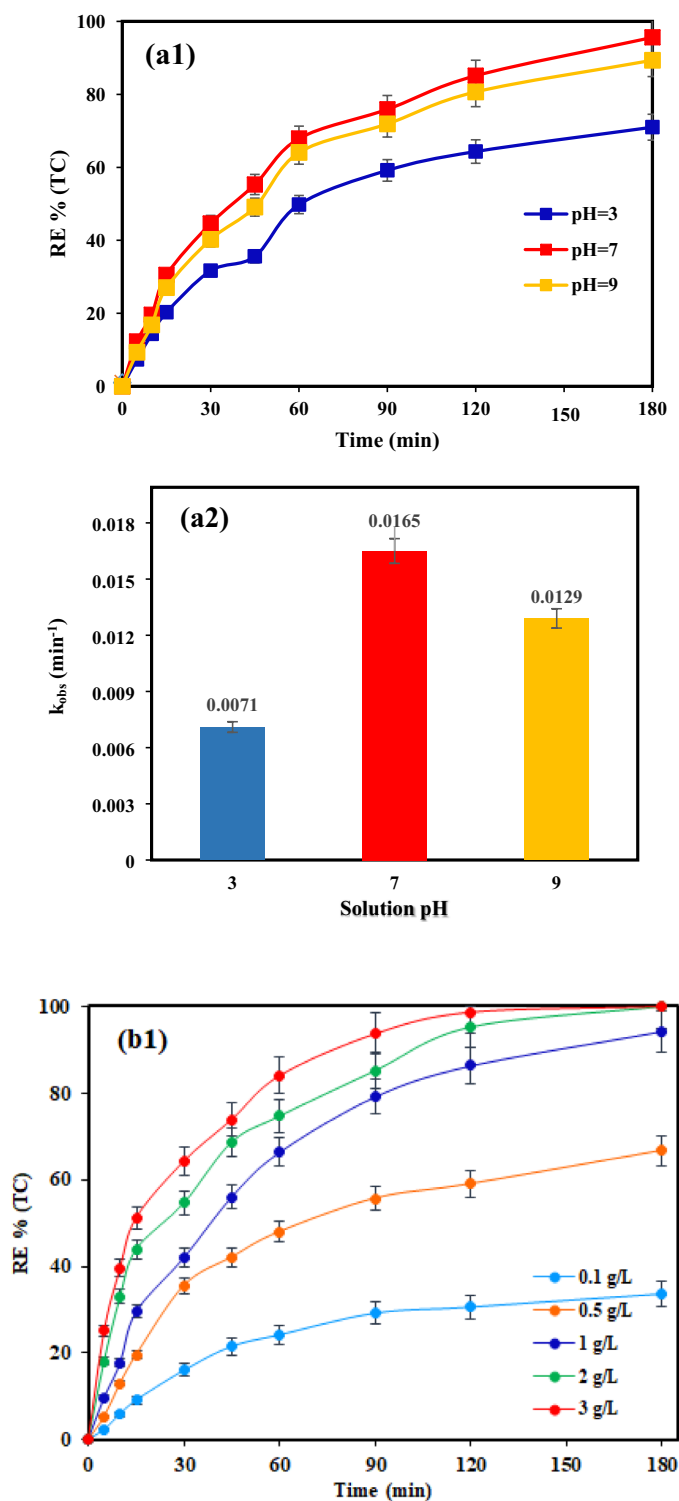


Figure 5. Effects of operational parameters and variation profiles of pseudo-first-order rate constants of TC degradation: (a) initial pH; (b) catalyst dose; (c) light intensity; (d) TC concentration (Reaction conditions: (a): catalyst dose = 1 g/L, [TC] = 30 mg/L and light intensity = 60 mW/cm²; (b): ([TC] = 30 mg/L, pH = 7 and light intensity = 60 mW/cm²; (c): [TC] = 30 mg/L, pH = 7 and catalyst dose = 2 g/L; (d): pH = 7 and catalyst dose = 2 g/L and light intensity = 60 mW/cm²).

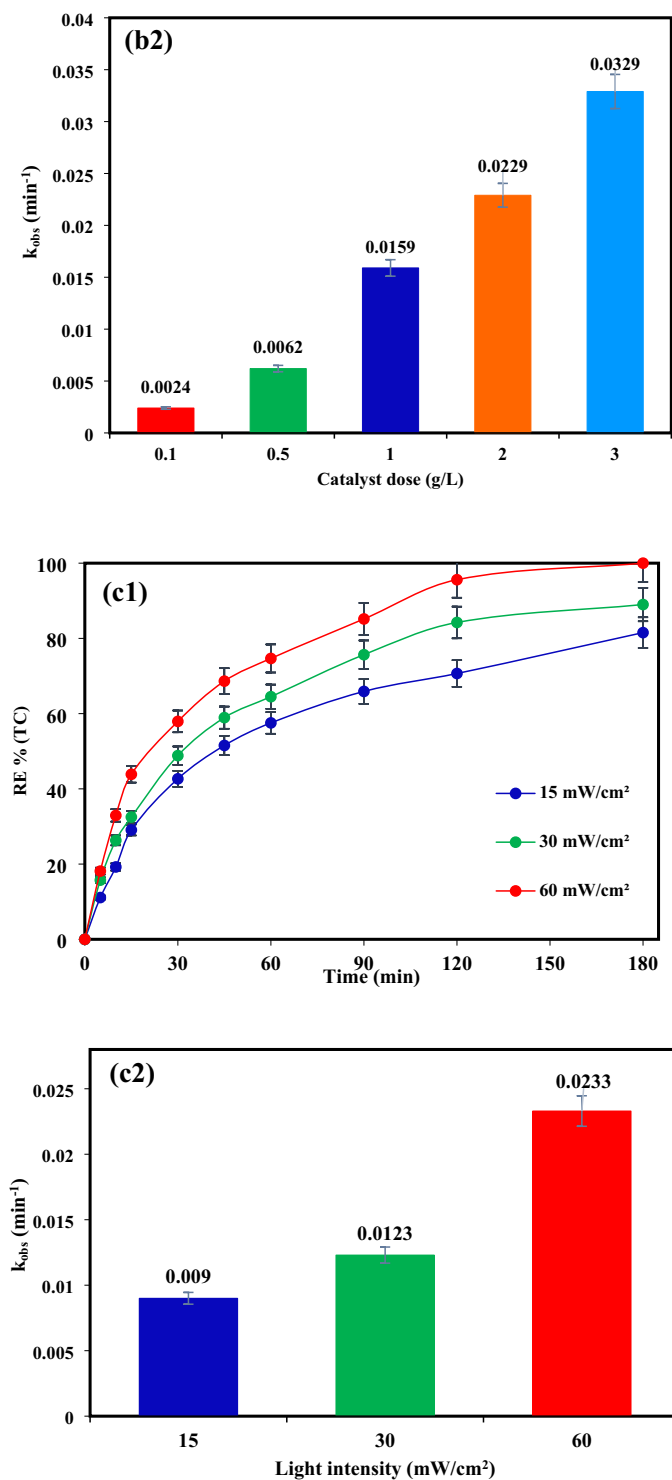


Figure 5. (continued)

an increase in catalyst dosage from 0.1 to 3 g/L resulted in a rise in the reaction rate constant (k_{obs}) from 0.0024 to 0.0329 min^{-1} .

The rise in active sites on the photocatalyst surface is believed to be the cause of the observed phenomenon⁶³. However, adding a photocatalyst dosage more than 2 g/L had no significant effect on degradation efficiency. Therefore, according to economic considerations and appropriate degradation efficacy, the quantity of 2 g/L of TiO_2/NP was determined as the optimal value for further photocatalytic experiments.

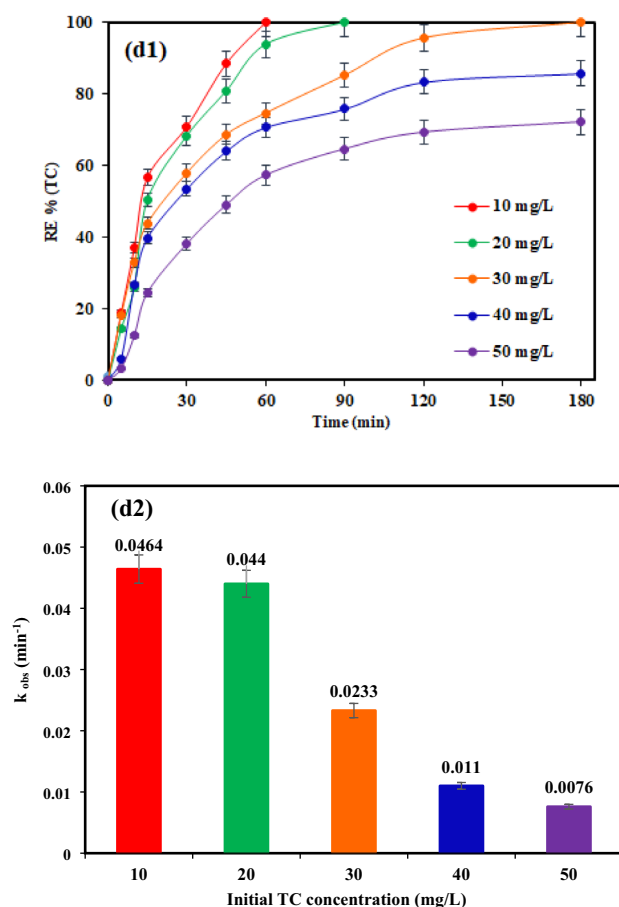


Figure 5. (continued)

On the one hand, when the concentration of the photocatalyst is increased, it leads to an expansion of its surface area and a rise in the quantity of active sites. Consequently, a higher quantity of pollutant molecules and light photons can attach to the photocatalyst surface, increasing electron excitation from the valence band to the conduction band¹. Furthermore, the amount of $\cdot\text{OH}$ and superoxide radicals that enhances the photocatalytic reaction could undergo an increase^{5,64}.

On the other hand, at higher photocatalyst dosage, the augmented opacity of the solution impedes the infiltration of light on the surface of the photocatalyst³⁸. Also, an overabundance of light scattering resulted in a decline in the $\cdot\text{OH}$ generation, ultimately resulting in a decrease in the photocatalytic efficacy⁶⁴. Furthermore, catalyst loading on the surface beyond the optimum led to agglomeration of catalyst^{4,61}. Thereby, the active sites of the catalyst surface become inaccessible for pollutants and photons absorption.

Ahmadi et al. (2017) discovered that the dosage of the catalyst can have both positive and negative impacts on phenol degradation in the photocatalytic approach. According to the findings of their study, the elimination efficiency of phenol was enhanced after 100 min when the concentration of MWCNT/TiO₂ nanocomposite was raised from 0.1 to 2 g/L. However, no rise in removal efficiency was observed when the concentration was set at 4 g/L, at the same reaction time. The researchers suggested that increasing the concentration of the catalyst could reduce active site access to light photons, resulting in a loss in photocatalyst overall efficiency⁶¹.

Influence of visible light intensity

The effectiveness of photocatalytic elimination of pollutants is significantly influenced by the intensity of light. At optimal catalyst concentration, the influence of various visible light intensities (15, 30, and 60 mW/cm^2) for TC removal was examined. As shown in Fig. 5 (c1,c2), by raising the irradiation intensity from 15–60 mW/cm^2 , the TC removal efficiency has improved from 82 (with the $k_{obs} = 0.009 \text{ min}^{-1}$) to 100% (with the $k_{obs} = 0.0233 \text{ min}^{-1}$) after 180 min. According to the results, TC degradation is positively impacted by light intensity. Because light intensity is required for the photochemical reaction to begin, electron–hole pairs (e^-/h^+) production predominates and electron–hole recombination is insignificant at higher light intensities^{64,65}. Furthermore, the number of light photons at higher intensity increased, which can also increase the photocatalytic decomposition of TC^{5,66}. Nevertheless, the lower decomposition efficiency observed at lower light intensity can be assigned to the competition between the separation of e^-/h^+ pairs and their recombination. This competition results in reduced ROS formation and as a consequence less degradation of contaminants⁶⁷.

Influence of TC concentration

Experiments were conducted under ideal conditions with varied TC concentrations ranging from 10 to 50 mg/L to evaluate the influence of the initial concentration of TC on the photocatalytic effectiveness of TiO₂/NP. The efficacy of TC removal diminished as the initial concentration increased, as depicted in Fig. 5(d1). This decrease was further supported by the decline in k_{obs} values (Fig. 5d2) from 0.0464 to 0.0076 min⁻¹ when the concentration of TC was elevated from 10 to 50 mg/L.

The reduction of active sites on the catalyst surface may be responsible for this phenomenon. When the catalyst dosage is kept constant, the quantity of active sites on the catalyst surface remains unchanged³⁸.

As the amount of pollutants increases, so does the number of pollutant molecules that may be present on the active sites of the catalyst surface. Consequently, the availability of active sites for this higher number of pollutant molecules will be less^{6,64}. In addition, as the concentration of pollutant increase, more TC molecules or the formed intermediates could be adsorbed on the photocatalyst surface. Therefore, more active oxidant species are required to remove this high pollutant concentration, and their insufficiency escalates proportionally with the augmentation of TC amount^{4,61}. Conversely, Wang et al. (2020) suggested that an overabundance of pollutants adsorbed onto the photocatalyst surface can impede the transmission of optical photons to the photocatalysts surface. Thereby, the efficacy of the photocatalytic process is impeded by the deficiency of active oxidants including hydroxyl radicals and superoxide anions (O₂⁻)⁵⁹.

Performance of various processes on TC removal

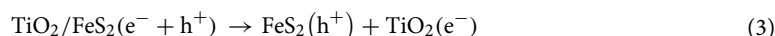
To examine the efficacy of TiO₂ or pyrite in TC removal, photocatalytic experiments were conducted in the presence of TiO₂ and pyrite alone at optimal conditions (pH 7, catalyst dosage of 2 g/L, TC concentration of 30 mg/L, and light intensity 60 mW/cm²), findings were subsequently compared with those of the TiO₂/NP system. Moreover, the impact of TiO₂/pyrite on TC elimination was explored in the absence of light. As demonstrated in Fig. 6a, the binding of TC on the TiO₂/NP surface could explain the elimination of TC in the absence of visible light. After 180 min of reaction time in a TiO₂-based system, TC elimination effectiveness was 63.54%. Meanwhile, a single pyrite system exhibited higher removal efficiency of 77.87% for TC throughout the same reaction time. On the contrary, coating TiO₂ on the surface of pyrite (Fig. 7) resulted in higher photocatalytic efficiency than in the presence of TiO₂ and pyrite alone. Also, as it can be seen, the efficiency of pyrite in photocatalytic removal of TC is greater than that of TiO₂. The dissimilarity between the band gaps of TiO₂ (3.2 eV)⁵⁹ and pyrite (0.95 eV)^{35,68}, which causes a difference in the absorption of light photons and more oxidant species generation in the photocatalytic process in the attendance of pyrite, may be the cause of the differences in removal efficiencies between these two substances³⁵. Indeed, the higher Fermi level of pyrite compared to TiO₂ causes electrons to transfer from pyrite to TiO₂ leading to an internal electric field between pyrite and TiO₂. Under the illumination of light, in accordance with the S-scheme photocatalyst approach, pyrite functions as the reduction photocatalyst (RP), while TiO₂ acts as the oxidation photocatalyst (OP). As a result, the photogenerated electrons gather in the conduction band (CB) of pyrite, while the photogenerated holes accumulate in the valence band (VB) of TiO₂. This process reduces the recombination of electron-hole pairs with a high potential, thereby enhancing the photocatalytic activity of the TiO₂/NP nanocomposite. Additionally, the low potential photogenerated holes in the valence band of pyrite are recombined by the photogenerated electrons in the conduction band of TiO₂, facilitated by the internal electric field. Consequently, the photogenerated electrons in the conduction band of pyrite and the holes in the valence band of TiO₂ are effectively utilized for TC reduction, resulting in a higher photocatalytic efficiency of TiO₂/NP for TC degradation⁶⁹⁻⁷¹.

In addition, the increased efficacy of pyrite in TC removal compared to TiO₂ can be described by the formation of ferrous ions^{57,72}. According to the following equation (Eq. (1)), first, the Fe in the solution is in a state of Fe(OH)²⁺. Under the irradiation of light, it is converted into the forms of Fe²⁺ and ·OH, thus providing one of the essential oxidant species for photocatalytic oxidation.



As observed in Fig. 6b, the reaction rate constant of TC decomposition was significantly rose in TiO₂/NP system under visible light irradiation (0.0233 min⁻¹).

As mentioned above, since pyrite has a relatively small band gap, the immobilization of TiO₂ on pyrite causes an improvement in the photocatalytic efficacy of TiO₂ during visible light exposure. In the conduction and valence bands of pyrite, photoelectrons (e⁻) and positive holes (h⁺) are produced under visible light, respectively^{52,73}. Furthermore, the H⁺ and ·OH radicals can be generated as a result of H₂O and positive holes (h⁺) reaction. (Eqs. (2)–(8))³⁵. Therefore, the existence of pyrite and TiO₂ causes the formation of additional oxidative species, which improves the effectiveness of TC removal⁷⁴. The TiO₂/NP photocatalytic efficiency was compared with previously researched photocatalysts, as demonstrated in Table 3.



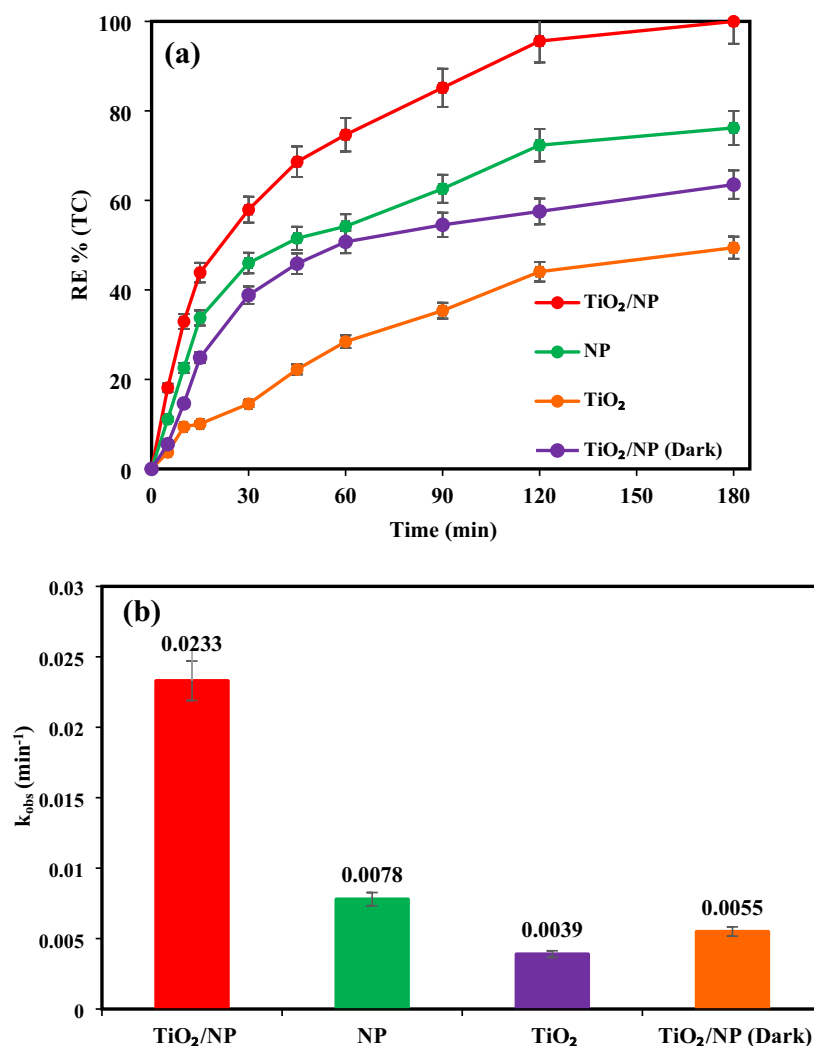


Figure 6. (a) TC Removal efficiency under different systems at optimal conditions ([TC] = 30 mg/L, pH = 7, catalyst dose = 2 g/L and light intensity = 60 mW/cm²), (b) variation profiles of pseudo-first-order rate constants of TC degradation.

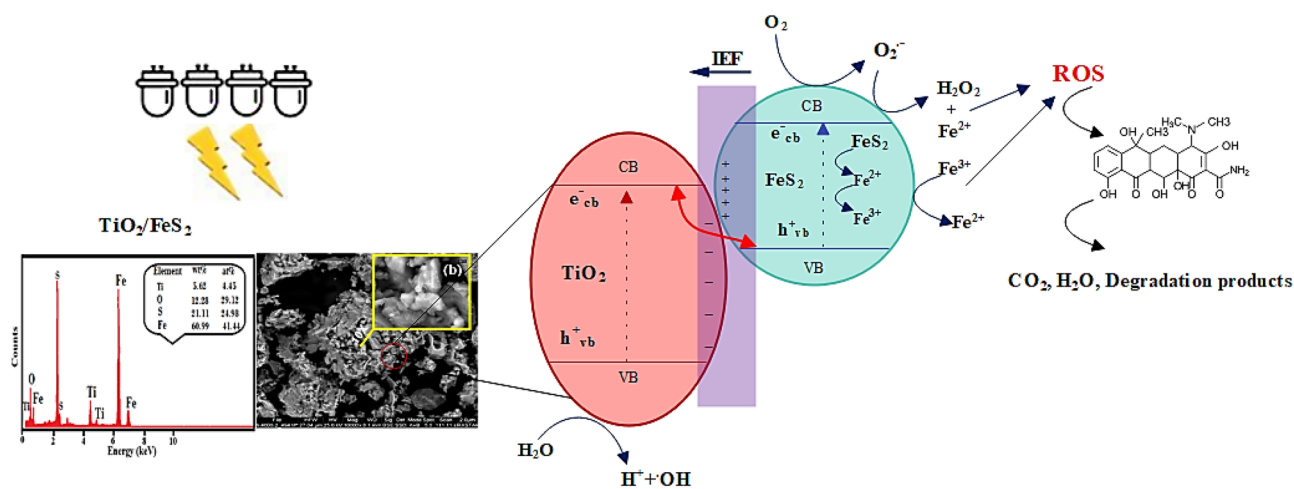


Figure 7. The schematic illustration of photocatalytic degradation of TC using TiO₂/NP.

No	Catalyst	Light source	Experimental conditions	Efficiency (%)	Ref
1	C ₃ N ₄ -TE@TiO ₂ /UiO-66	Visible light	[C ₀]:20 mg/L, [catalyst]: 0.4 g/L, [pH]:4, [Time]:40 min	96	26
2	Fe-MOF/CM	Visible light	[C ₀]:10 ppm, [catalyst]:0.375 g/L, [Time]:60 min	100	75
3	FeNi ₃ @SiO ₂ @TiO ₂	UV-light	[C ₀]:10 mg/L, [catalyst]: 0.005 g/L,[pH]:9, [Time]:200 min	100	1
4	Calcite/TiO ₂	UV-light	[C ₀]:50 mg/L, [catalyst]:1.5 g/L, [pH]:7, [Time]:300 min	>90	16
5	TiO ₂ /Mo ₉ O ₂₈ -BMPP	Visible light	[C ₀]:25 mg/L, [catalyst]: 0.15 g, [pH]:7, [Time]:115 min	97	59
6	MWCNT/TiO ₂	UVC-light	[C ₀]:10 mg/L, [catalyst]: 0.2 g/L, [pH]:5, [Time]:300 min	100	61
7	TiO ₂	Visible light	[C ₀]:10 mg/L, [catalyst]: 0.2 g/L, [Time]: 120 min	56.7	23
8	AgI/UiO-66(NH ₂)	Visible light	[C ₀]:10 mg/L, [catalyst]: 0.3 g/L, [pH]:4.3, [Time]:40 min	80.7	6
9	In-doped Mn ₂ O ₃	Visible light	[C ₀]:50 mg/L, [catalyst]:10 mg/L, [pH]:7, [Time]:180 min	93	63
10	MoS ₂ /ZnSnO ₃	Visible light	[C ₀]:30 mg/L, [catalyst]:0.25 g/L, [Time]:60 min	80.2	18
11	BiVO ₄ /FeVO ₄ @rGO	Visible light	[C ₀]:30 mg/L, [catalyst]:25 mg, [pH]:2, [Time]:100 min	91.5	76
12	Ag ₃ PO ₄ /AgBr/g-C ₃ N ₄	Visible light	[C ₀]:10 mg/L, [catalyst]:0.5 g/L, [pH]:7, [Time]:10 min	90	77
			[C ₀]:40 mg/L, [catalyst]:0.5 g/L, [pH]:7, [Time]:25 min	80.2	
13	AgBr-TiO ₂ -Pal	Visible light	[C ₀]:10 mg/L, [catalyst]:0.5 g/L, [pH]:9, [Time]:90 min	90	22
14	CDs-ZnSnO ₃	Visible light	[C ₀]:10 mg/L, [catalyst]:0.25 g/L, [Time]:60 min	81.7	78
15	TiO ₂ /NP	Visible light	[C ₀]:30 mg/L, [catalyst]:2 g/L, [pH]:7, [Time]:180 min	100	This study

Table 3. Comparison of TC photocatalytic removal using the different photocatalyst.



Reactive species identification

The effectiveness of the photocatalytic system is significantly influenced by the presence of oxidative species. To determine the most significant reactive oxidation species, quenching agents such as TBA, KI, and Cr (VI) with a concentration of 0.5 mM were utilized as scavengers of $\cdot\text{OH}$, h^+ , and e^- , respectively. As presented in Fig. 8a, in the absence of scavengers, 95.6% of the target compound (TC) was eliminated within 120 min of photocatalytic treatment. Nevertheless, the removal efficacy of TC declined in the attendance of all radical scavengers. The presence of TBA causes a remarkable reduction in the removal efficacy of TC, with a reaction rate constant (k_{obs}) (Fig. 8b) of 0.0042 min^{-1} . This suggests that hydroxyl radicals ($\cdot\text{OH}$) are the primary oxidative species involved in the photocatalytic decomposition of TC, compared to other active species.

This data implies that the attendance of TBA reduced the photocatalytic system's efficacy, underlining that $\cdot\text{OH}$ radicals are major involved ROS in the elimination of TC^{57,79}. The observed effect may be due to TBA's increased aqueous solubility and lower absorption rate by the catalyst, allowing it to swiftly scavenge free radicals⁸⁰. Hence, $\cdot\text{OH} > \text{h}^+ > \text{e}^-$ are the influential oxidation species participating in the photocatalytic elimination of TC by TiO₂/NP composite.

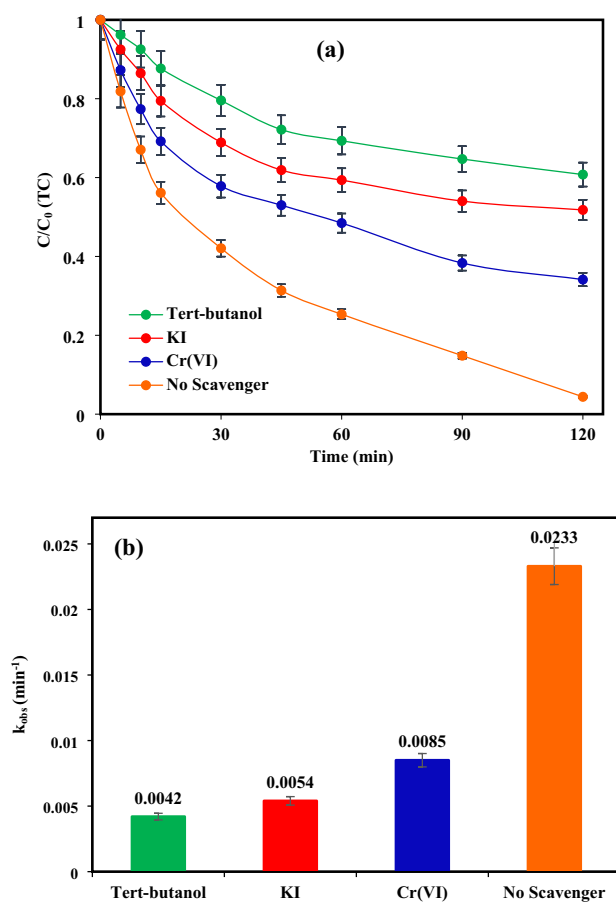


Figure 8. (a) The influence of various scavengers and (b) the reaction rate constants associated with those scavengers under ideal circumstances ($[TC] = 30 \text{ mg/L}$, $\text{pH} = 7$, catalyst dose = 2 g/L and light intensity = 60 mW/cm^2).

Effects of inorganic ions on TC removal

Since the practical application of photocatalytic oxidation may be influenced by inorganic ions, which widely exist in aqueous matrices, indeed, the photocatalytic efficiency of a TiO_2/NP system for TC removal was evaluated under optimal conditions in the existence of Ca^{2+} , NO_3^- , SO_4^{2-} , and Cl^- ions at a concentration of 20 mM . According to the results (Fig. 9 (a,b)), it can be observed that the attendance of different ions has resulted in a decrease in the removal of TC in comparison to water without ions. Furthermore, the restrictive impact of these ions has been observed to follow the order of $\text{Ca}^{2+} > \text{NO}_3^- > \text{Cl}^- > \text{SO}_4^{2-}$. This phenomenon is caused by the assimilation of light photons by these ions, which impede the photolysis of additional water molecules and the establishment of hydroxyl radicals. Consequently, the quantity of $\cdot\text{OH}$ radicals available for the oxidation of TC is reduced. This is because the scavenging agents (such as TBA, KI, and Cr(VI)) react with the $\cdot\text{OH}$ radicals, resulting in a decline in their concentration and subsequent reduction in the overall efficacy of the photocatalytic system⁸¹. Furthermore, the existence of inorganic ions may lead to the occupation of active sites present on the TiO_2/NP surface, which can result in a decline in the accessibility of TC molecules due to competition with these ions. This causes a decline in the photocatalytic efficacy of the system since fewer active sites are obtainable for the oxidation of TC molecules⁷⁹. Conversely, the reaction of ions with the main reactive species ($\cdot\text{OH}$, h^+), which leads to the generation of radicals with lower oxidative potential, can be another reason for the reduction in the oxidation process^{79,82}.

As shown, the highest hindering effect was related to calcium ions, possibly due to the consumption of hydroxyl ions and bonding with ferrous ions⁸³. The addition of nitrate ions significantly reduces TC elimination because these ions have a radical scavenging function and produce low oxidative species such as NO_3^{\cdot} and NO_2^{\cdot} (Eqs. (9) and (10))⁸⁴.



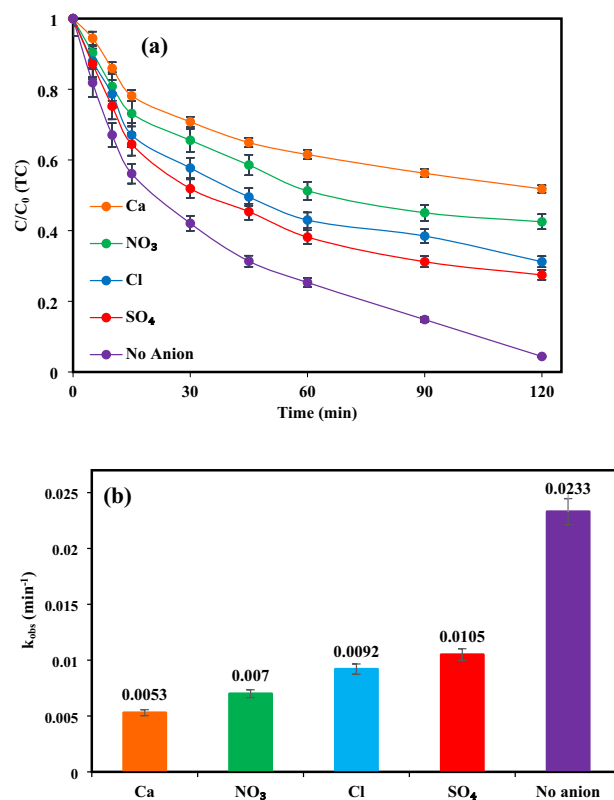


Figure 9. (a) TC Removal rate and (b) the corresponding reaction rate constants at optimum conditions ([TC] = 30 mg/L, pH = 7, catalyst dose = 2 g/L and light intensity = 60 mW/cm²).

Moreover, similar scavenging effects are due to the high proclivity of chlorine ions to combine with $\cdot\text{OH}$ radicals and positive holes on TiO_2/NP surface lead to generating lower reactive species (Eqs. (10)–(17)). On the other hand, the hindrance of TC molecule accessibility to $\cdot\text{OH}$ radicals due to the competition of pollutant molecules with these ions for reaction with $\cdot\text{OH}$ radicals may be a contributing cause for the declined efficacy observed in the presence of chloride⁸⁵.



The findings indicate that the existence of sulfate ions resulted in the least inhibitory effect, possibly due to the interaction with active species and subsequent formation of SO_4^\cdot radicals possessing a greater redox potential (2.5–3.1 eV) than $\cdot\text{OH}$ radicals (Eqs. (19), (20))⁸⁵.





Mineralization and reusability of TiO₂/pyrite

Complete removal of TC does not mean that mineralization has been completed, and CO₂ and H₂O have been produced, so in this work, the mineralization of TC by the TiO₂/NP system was investigated by measuring TOC elimination. Figure 10 demonstrates that, considering optimal circumstances, TC was entirely eliminated within 180 min, while TOC removal reached 84%. This suggests that the entire mineralization of TC during the TiO₂/NP photocatalytic process required longer reaction times compared to the photocatalytic removal of TC. This phenomenon may arise as a result of the manufacturing of diverse products and their competing with TC molecules^{61,80}.

The durability and reusability of the catalyst are crucial variables in selecting and application of the catalyst for full scale. Herein, the reusability of TiO₂/NP nanocomposite was examined during fourth repetitive runs under optimum conditions. By completing each run, the catalyst was isolated from the solution, rinsed with water, and subsequently stored at 90 °C for 4 h for the subsequent run. As depicted in Fig. 11a, only an 8% decrease in the efficiency of TC removal occurred following four cycles of catalyst utilization. Therefore, it indicated the nanocomposites high reusability and good photocatalytic activity. Nonetheless, the slight decrease in elimination effectiveness may be ascribed to the by-product formation during the elimination process, which could accumulate on the nanocomposite surface and obstruct the active sites on the catalyst surface, thereby hindering the removal of TC⁸⁶. Furthermore, the photocatalytic efficiency of TiO₂/NP probably declined due to the nanocomposite surface passivation and the number of ferrous ions released from the pyrite, which occurred after multiple uses of the catalyst⁸⁷. Moreover, XRD analysis was used to further investigate the stability of the photocatalyst. The XRD pattern (Fig. 11b) indicated that the XRD peaks of the fresh and used photocatalyst are relatively constant, with a slight decrease in peak intensity due to minimal Fe leaching. The results indicated that the release of Fe was 0.134 mg/L after 4 cycles, confirming the high physicochemical stability of the photocatalyst, as the leaching of metals was less than 0.25 mg/L, demonstrating the proper stability of the photocatalyst⁸⁸.

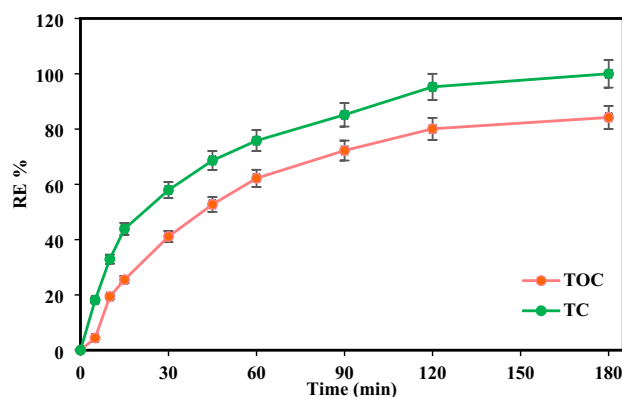


Figure 10. Removal efficiency of TOC by TiO₂/NP at optimum conditions ([TC] = 30 mg/L, pH = 7, catalyst doe = 2 g/L and light intensity = 60 mW/cm²).

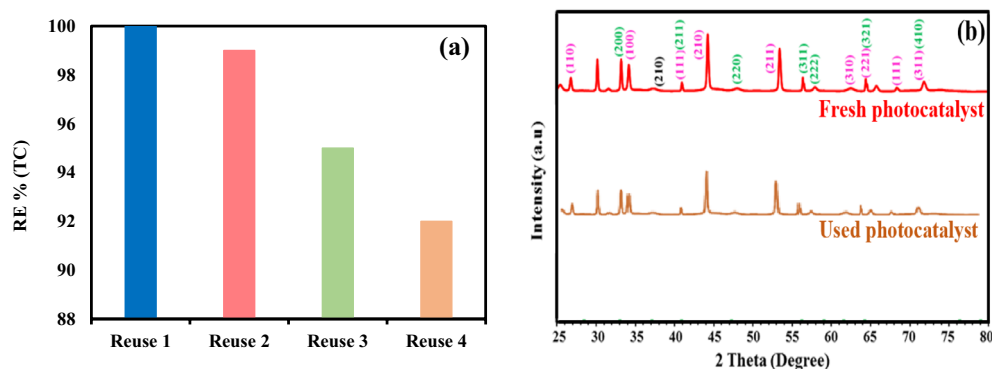


Figure 11. (a) the reusability of TiO₂/NP at optimum conditions ([TC] = 30 mg/L, pH = 7, catalyst doe = 2 g/L and light intensity = 60 mW/cm²) (b) XRD pattern of fresh and used photocatalyst.

Possible tetracycline photocatalytic degradation pathways

The photocatalytic breakdown of TC varies according to the type of photocatalyst and reaction conditions, leading to the formation of diverse by-products. Many studies showed that TC is generally converted into short-chain compounds and finally H_2O and CO_2 under various chemical processes such as dealkylation, hydroxylation, and ring opening^{89,90}. The proposed pathway of TC decomposition in present work (Fig. 12) is based on the pathways proposed in previous studies related to the photocatalytic decomposition of TC in TiO_2 -based systems.

In one pathway, TC undergoes various reactions such as dealkylation and demethylation, as a result, some intermediates may be generated due to the elimination of functional groups with low binding energy such as dimethylamine^{23,80}. Many studies have shown that in this pathway an intermediate with m/z 431 is generated, subsequently other intermediates with m/z 417, 400, 373, 339 are produced^{91,92}. Further oxidation in the attendance of ROS including $\cdot OH$, $\cdot O_2^-$ and h^+ , leads to the generation of smaller intermediates through ring opening and central carbon cleavage reactions. These byproducts can be more oxidized to produce tiny organic molecules including organic acids, alcohols, H_2O , and CO_2 ^{93,94}.

In another pathway, the attendance of a weak π bond in the TC structure facilitates the addition of hydroxyl groups through a hydroxylation process. This leads to the origination of the main intermediate with $m/z = 461$ ⁹⁵. Further, by adding more hydroxyl groups, the mass-to-charge ratio increases, and other intermediates with m/z 475 and 495 are produced⁸⁰. The addition of hydroxyl groups in the structure of TC causes the double bond in

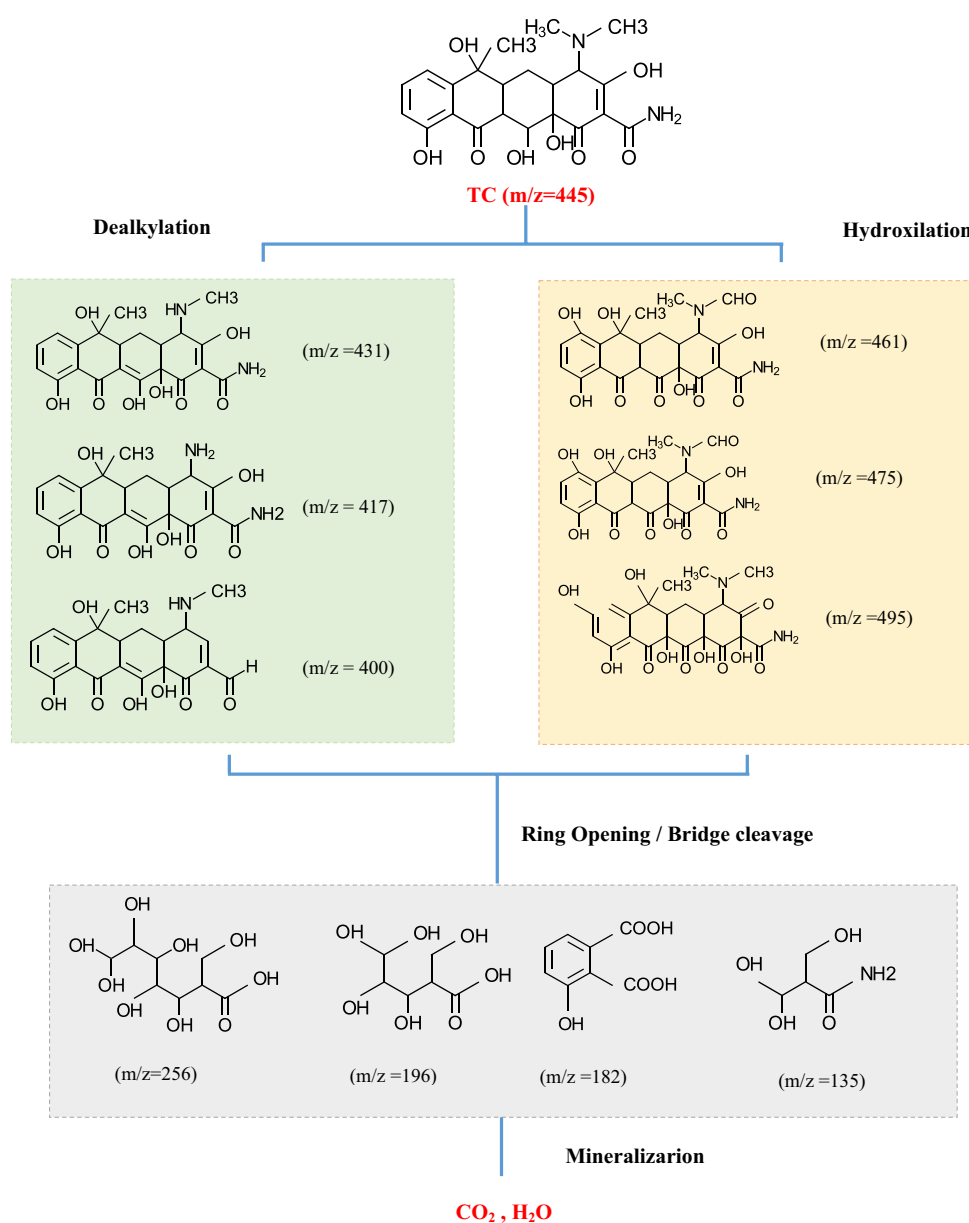


Figure 12. Feasible photocatalytic degradation pathways of TC in TiO_2/NP system.

its structure to be destroyed, subsequently, with the attack of more oxidant species, intermediates with a lower number of rings with m/z 256, 196, 182, 135 are generated^{91,92,96,97}. Generally, during the hydroxylation process and after adding OH in the tetracycline structure through oxidation and mineralization mechanisms, the aromatic ring undergoes breakage, resulting in the establishment of intermediates, as well as the production of CO₂, H₂O, and inorganic ions.

Conclusion

The current work looked into the photocatalytic effectiveness of synthesized TiO₂/NP for the decomposing of TC under visible light exposure. The findings suggest that the prepared nanocomposite demonstrated effective performance in removing TC from the aqueous solution, so that 100% of TC was removed under optimal conditions within 180 min reaction time. However, the photocatalytic activity of catalyst could be changed by variation in experimental conditions. The removal rate was accelerated by increased light intensity and the addition of optimum TiO₂/NP dosage. Nevertheless, subsequent increases in the dosage of nanocomposite reduced the photocatalytic efficacy due to the agglomeration of catalysts and shortage of active sites to adsorb pollutants. Furthermore, photocatalytic process had lower efficiency by increasing the TC concentration. The predominant reactive oxidation species identified by adding quenching agents were hydroxyl radicals, which were crucial for photocatalytic activity. Also, reusability experiments of the TiO₂/NP revealed that after four cycles, the photocatalytic efficiency does not significantly decline. Generally, it can be concluded that the TiO₂/NP system had a suitable efficiency under optimized experimental conditions for TC removal. However, since the present investigation was conducted at a lab scale on synthetic effluent, the photocatalytic efficiency may differ from actual wastewater. Therefore, further studies are suggested to evaluate this photocatalytic process at a pilot scale using wastewater effluent.

Data availability

All data generated or analysed during this study are included in this published article.

Received: 9 December 2023; Accepted: 14 February 2024

Published online: 29 February 2024

References

1. Khodadadi, M., Ehrampoush, M., Ghaneian, M., Allahresani, A. & Mahvi, A. Synthesis and characterizations of FeNi₃@ SiO₂@ TiO₂ nanocomposite and its application in photo-catalytic degradation of tetracycline in simulated wastewater. *J. Mol. Liq.* **255**, 224–232 (2018).
2. Drogue, C. *et al.* Treatment of antibiotic cephalixin by heterogeneous electrochemical Fenton-based processes using chalcopyrite as sustainable catalyst. *Sci. Total Environ.* **740**, 140154 (2020).
3. Qu, L. *et al.* Nanospherical composite of WO₃ wrapped NaTaO₃: Improved photodegradation of tetracycline under visible light irradiation. *Appl. Surf. Sci.* **388**, 412–419 (2016).
4. Moradi, M. *et al.* CuO and ZnO co-anchored on g-C₃N₄ nanosheets as an affordable double Z-scheme nanocomposite for photocatalytic decontamination of amoxicillin. *Appl. Catal. B* **285**, 119838 (2021).
5. Isari, A. A. *et al.* Sono-photocatalytic degradation of tetracycline and pharmaceutical wastewater using WO₃/CNT heterojunction nanocomposite under US and visible light irradiations: A novel hybrid system. *J. Hazard. Mater.* **390**, 122050 (2020).
6. Pan, Y. *et al.* Stable self-assembly AgI/UiO-66 (NH₂) heterojunction as efficient visible-light responsive photocatalyst for tetracycline degradation and mechanism insight. *Chem. Eng. J.* **384**, 123310 (2020).
7. Khataee, A., Fathinia, S. & Fathinia, M. Production of pyrite nanoparticles using high energy planetary ball milling for sonocatalytic degradation of sulfasalazine. *Ultrason. Sonochem.* **34**, 904–915 (2017).
8. Hoseini, M., Kamani, H., Jaafari, J. & Mahvi, A. Photocatalytic Degradation of Tetracycline Using Nanosized Titanium Dioxide in Aqueous Solution.
9. Javid, A. *et al.* Assessment of tetracycline contamination in surface and groundwater resources proximal to animal farming houses in Tehran, Iran. *J. Environ. Health Sci. Eng.* **14**, 1–5 (2016).
10. Liu, X., Lu, S., Meng, W. & Wang, W. Occurrence, source, and ecological risk of antibiotics in Dongting Lake, China. *Environ. Sci. Pollut. Res.* **25**, 11063–11073 (2018).
11. Xu, L. *et al.* Occurrence, fate, and risk assessment of typical tetracycline antibiotics in the aquatic environment: A review. *Sci. Total Environ.* **753**, 141975 (2021).
12. Mengting, Z. *et al.* Applicability of TiO₂ (B) nanosheets@ hydrochar composites for adsorption of tetracycline (TC) from contaminated water. *J. Hazard. Mater.* **405**, 123999 (2021).
13. Qin, K. *et al.* Removal trends of sulfonamides and their ARGs during soil aquifer treatment and subsequent chlorination: Effect of aerobic and anaerobic biodegradation. *Environ. Sci. Water Res. Technol.* **6**, 2331–2340 (2020).
14. Du, X. *et al.* Removal of manganese, ferrous and antibiotics from groundwater simultaneously using peroxydisulfate-assisted in-situ oxidation/coagulation integrated with ceramic membrane process. *Separ. Purif. Technol.* **252**, 117492 (2020).
15. Borba, F. H. *et al.* Genotoxicity and by-products assessment in degradation and mineralization of Ciprofloxacin by UV/H₂O₂ process. *J. Environ. Chem. Eng.* **6**, 6979–6988 (2018).
16. Belhouche, N., Hamdi, B., Chenchouni, H. & Bessekhouad, Y. Photocatalytic degradation of tetracycline antibiotic using new calcite/titania nanocomposites. *J. Photochem. Photobiol. A Chem.* **372**, 196–205 (2019).
17. de Luna, M. D. G., Paragas, L. K. B. & Doong, R.-A. Insights into the rapid elimination of antibiotics from aqueous media by tunable C₃N₄ photocatalysts: Effects of dopant amount, co-existing ions and reactive oxygen species. *Sci. Total Environ.* **669**, 1053–1061 (2019).
18. Guo, F. *et al.* MoS₂ nanosheets anchored on porous ZnSnO₃ cubes as an efficient visible-light-driven composite photocatalyst for the degradation of tetracycline and mechanism insight. *J. Hazard. Mater.* **390**, 122158 (2020).
19. Liu, S., Jiang, X., Waterhouse, G. I., Zhang, Z.-M. & Yu, L.-M. Construction of Z-scheme Titanium-MOF/plasmonic silver nanoparticle/NiFe layered double hydroxide photocatalysts with enhanced dye and antibiotic degradation activity under visible light. *Separ. Purif. Technol.* **278**, 119525 (2021).
20. Li, S., Dong, K., Cai, M., Li, X. & Chen, X. A plasmonic S-scheme Au/MIL-101 (Fe)/BiOBr photocatalyst for efficient synchronous decontamination of Cr (VI) and norfloxacin antibiotic. *eScience* <https://doi.org/10.1016/j.esci.2023.100208> (2023).
21. Li, S. *et al.* Enhanced antibiotic degradation performance of Cd_{0.5}Zn_{0.5}/Bi₂MoO₆ S-scheme photocatalyst by carbon dot modification. *J. Mater. Sci. Technol.* **164**, 59–67. <https://doi.org/10.1016/j.jmst.2023.05.009> (2023).

22. Shi, Y. *et al.* Visible-light-driven AgBr–TiO₂-Palygorskite photocatalyst with excellent photocatalytic activity for tetracycline hydrochloride. *J. Clean. Prod.* **277**, 124021. <https://doi.org/10.1016/j.jclepro.2020.124021> (2020).
23. Wu, S., Hu, H., Lin, Y., Zhang, J. & Hu, Y. H. Visible light photocatalytic degradation of tetracycline over TiO₂. *Chem. Eng. J.* **382**, 122842 (2020).
24. Martins, A. C. *et al.* Sol-gel synthesis of new TiO₂/activated carbon photocatalyst and its application for degradation of tetracycline. *Ceram. Int.* **43**, 4411–4418. <https://doi.org/10.1016/j.ceramint.2016.12.088> (2017).
25. Ma, Z. *et al.* A high-performance photocatalyst of ZnTCPP sensitized porous graphitic carbon nitride for antibiotic degradation under visible light irradiation. *Appl. Surf. Sci.* **484**, 489–500 (2019).
26. Safaralizadeh, E., Mahjoub, A. R., Fazlali, F. & Bagheri, H. Facile construction of C₃N₄-TE@ TiO₂/UiO-66 with double Z-scheme structure as high performance photocatalyst for degradation of tetracycline. *Ceram. Int.* **47**, 2374–2387 (2021).
27. Tiwari, A., Shukla, A., Tiwari, D. & Lee, S. M. Nanocomposite thin films Ag₀(NP)/TiO₂ in the efficient removal of micro-pollutants from aqueous solutions: A case study of tetracycline and sulfamethoxazole removal. *J. Environ. Manag.* **220**, 96–108. <https://doi.org/10.1016/j.jenvman.2018.05.019> (2018).
28. Cai, M., Liu, Y., Dong, K., Chen, X. & Li, S. Floatable S-scheme Bi₂WO₆/C₃N₄/carbon fiber cloth composite photocatalyst for efficient water decontamination. *Chin. J. Catal.* **52**, 239–251. [https://doi.org/10.1016/S1872-2067\(23\)64496-1](https://doi.org/10.1016/S1872-2067(23)64496-1) (2023).
29. Li, S. *et al.* Constructing Cd_{0.5}Zn_{0.5}/Bi₂WO₆ S-scheme heterojunction for boosted photocatalytic antibiotic oxidation and Cr(VI) reduction. *Adv. Powder Mater.* **2**, 100073. <https://doi.org/10.1016/j.apmate.2022.100073> (2023).
30. Xu, Q., Zhang, L., Cheng, B., Fan, J. & Yu, J. S-scheme heterojunction photocatalyst. *Chem* **6**, 1543–1559 (2020).
31. Xu, Q., Wageh, S., Al-Ghamdi, A. A. & Li, X. Design principle of S-scheme heterojunction photocatalyst. *J. Mater. Sci. Technol.* **124**, 171–173 (2022).
32. Al-Ghamdi, A. A., Jafer, R., Li, X. & Zhong, P. A new heterojunction in photocatalysis: S-scheme heterojunction. *Chin. J. Catal.* **42**, 667–669 (2021).
33. Feng, D., Li, X., Liu, Y., Chen, X. & Li, S. Emerging bismuth-based step-scheme heterojunction photocatalysts for energy and environmental applications. *Renewables* **1**, 485–513 (2023).
34. Moradi, M., Kalantary, R. R., Esrafil, A., Jafari, A. J. & Gholami, M. Visible light photocatalytic inactivation of *Escherichia coli* by natural pyrite assisted by oxalate at neutral pH. *J. Mol. Liquids* **248**, 880–889. <https://doi.org/10.1016/j.molliq.2017.10.115> (2017).
35. Moradi, M. *et al.* Visible-light-driven photocatalytic inactivation of *Escherichia coli* by titanium dioxide anchored on natural pyrite. *Inorg. Chem. Commun.* **144**, 109913. <https://doi.org/10.1016/j.inoche.2022.109913> (2022).
36. Li, Y. *et al.* Construction of S-scheme heterostructured TiO₂/g-C₃N₄ composite microspheres with sunlight-driven photocatalytic activity. *Mater. Today Commun.* **36**, 106431 (2023).
37. Ge-Ge, Z. *et al.* Enhancing photocatalytic pollutant degradation through S-scheme electron transfer and sulfur vacancies in BiFeO₃/ZnIn₂S₄ heterojunctions. *J. Compos. Sci.* **7**, 280 (2023).
38. Qian, S. *et al.* New insights on the enhanced non-hydroxyl radical contribution under copper promoted TiO₂/GO for the photo-degradation of tetracycline hydrochloride. *J. Environ. Sci.* **100**, 99–109 (2021).
39. Ghorbani, M., Solaimany Nazar, A. R., Frahadian, M. & Khosravi, M. Facile synthesis of Z-scheme ZnO-nanorod @ BiOBr-nanosheet heterojunction as efficient visible-light responsive photocatalyst: The effect of electrolyte and scavengers. *J. Photochem. Photobiol. A Chem.* **429**, 113930. <https://doi.org/10.1016/j.jphotochem.2022.113930> (2022).
40. Senasu, T., Nijpanich, S., Juabrum, S., Chanlek, N. & Nanan, S. Cds/BiOBr heterojunction photocatalyst with high performance for solar-light-driven degradation of ciprofloxacin and norfloxacin antibiotics. *Appl. Surf. Sci.* **567**, 150850 (2021).
41. Senasu, T., Youngme, S., Hemavibool, K. & Nanan, S. Sunlight-driven photodegradation of oxytetracycline antibiotic by BiVO₄ photocatalyst. *J. Solid State Chem.* **297**, 122088. <https://doi.org/10.1016/j.jssc.2021.122088> (2021).
42. Chankhanittha, T. *et al.* Silver decorated ZnO photocatalyst for effective removal of reactive red azo dye and ofloxacin antibiotic under solar light irradiation. *Colloids Surf. A Physicochem. Eng. Aspects* **626**, 127034 (2021).
43. Dhiman, P. *et al.* Solar active nano-Zn_{1-x}MgxFe₂O₄ as a magnetically separable sustainable photocatalyst for degradation of sulfadiazine antibiotic. *J. Mol. Liquids* **294**, 111574 (2019).
44. Aram, M. *et al.* Metronidazole and Cephalexin degradation by using of Urea/TiO₂/ZnFe₂O₄/Clinoptilolite catalyst under visible-light irradiation and ozone injection. *J. Mol. Liquids* **304**, 112764 (2020).
45. Li, S., Cai, M., Wang, C. & Liu, Y. Ta₃N₅/CdS core-shell S-scheme heterojunction nanofibers for efficient photocatalytic removal of antibiotic tetracycline and Cr(VI): Performance and mechanism insights. *Adv. Fiber Mater.* **5**, 994–1007. <https://doi.org/10.1007/s42765-022-00253-5> (2023).
46. Li, S. *et al.* MIL-101(Fe)/BiOBr S-scheme photocatalyst for promoting photocatalytic abatement of Cr(VI) and enrofloxacin antibiotic: Performance and mechanism. *Chin. J. Catal.* **51**, 101–112. [https://doi.org/10.1016/S1872-2067\(23\)64479-1](https://doi.org/10.1016/S1872-2067(23)64479-1) (2023).
47. Li, S. *et al.* S-scheme MIL-101 (Fe) octahedrons modified Bi₂WO₆ microspheres for photocatalytic decontamination of Cr (VI) and tetracycline hydrochloride: Synergistic insights, reaction pathways, and toxicity analysis. *Chem. Eng. J.* **455**, 140943 (2023).
48. Van Thuan, D. *et al.* Photodegradation of ciprofloxacin antibiotic in water by using ZnO-doped g-C₃N₄ photocatalyst. *Chemosphere* **308**, 136408 (2022).
49. Labiadh, L., Oturan, M. A., Panizza, M., Hamadi, N. B. & Ammar, S. Complete removal of AHPS synthetic dye from water using new electro-fenton oxidation catalyzed by natural pyrite as heterogeneous catalyst. *J. Hazard. Mater.* **297**, 34–41 (2015).
50. Gao, J. *et al.* Mechanisms for photo assisted Fenton of synthesized pyrrhotite at neutral pH. *Appl. Surf. Sci.* **463**, 863–871 (2019).
51. Chen, Y.-H. *et al.* Using the high-temperature phase transition of iron sulfide minerals as an indicator of fault slip temperature. *Sci. Rep.* **9**, 1–6 (2019).
52. Xin, Y., Li, Z., Wu, W., Fu, B. & Zhang, Z. Pyrite FeS₂ sensitized TiO₂ nanotube photoanode for boosting near-infrared light photoelectrochemical water splitting. *ACS Sustain. Chem. Eng.* **4**, 6659–6667 (2016).
53. Kalantary, R. R. *et al.* Enhanced photocatalytic inactivation of *E. coli* by natural pyrite in presence of citrate and EDTA as effective chelating agents: Experimental evaluation and kinetic and ANN models. *J. Environ. Chem. Eng.* **7**, 102906 (2019).
54. Guo, H.-X., Lin, K.-L., Zheng, Z.-S., Xiao, F.-B. & Li, S.-X. Sulfanilic acid-modified P25 TiO₂ nanoparticles with improved photocatalytic degradation on Congo red under visible light. *Dyes Pigments* **92**, 1278–1284 (2012).
55. Khataee, A., Gholami, P. & Sheydaei, M. Heterogeneous Fenton process by natural pyrite for removal of a textile dye from water: Effect of parameters and intermediate identification. *J. Taiwan Inst. Chem. Eng.* **58**, 366–373 (2016).
56. Razavi-Khosroshahi, H., Wenhao, S. & Fuji, M. Synthesis of TiO₂ hollow nanoparticles with different shell thickness and effect of structure on photocatalytic activity. *Solid State Sci.* **103**, 106179 (2020).
57. Mashayekh-Salehi, A. *et al.* Use of mine waste for H₂O₂-assisted heterogeneous Fenton-like degradation of tetracycline by natural pyrite nanoparticles: Catalyst characterization, degradation mechanism, operational parameters and cytotoxicity assessment. *J. Clean. Prod.* **291**, 125235 (2021).
58. Tang, T. *et al.* Novel pn heterojunction Bi₂O₃/Ti³⁺-TiO₂ photocatalyst enables the complete removal of tetracyclines under visible light. *Chem. Eng. J.* **417**, 128058 (2021).
59. Wang, X. *et al.* Preparation of 2D supramolecular material doping with TiO₂ for degradation of tetracycline. *Environ. Res.* **202**, 111689. <https://doi.org/10.1016/j.envres.2021.111689> (2021).
60. Zhang, M., Xu, L., Qi, C. & Zhang, M. Highly effective removal of tetracycline from water by hierarchical porous carbon: Batch and column adsorption. *Ind. Eng. Chem. Res.* **58**, 20036–20046. <https://doi.org/10.1021/acs.iecr.9b03547> (2019).

61. Ahmadi, M. *et al.* Enhanced photocatalytic degradation of tetracycline and real pharmaceutical wastewater using MWCNT/TiO₂ nano-composite. *J. Environ. Manag.* **186**, 55–63. <https://doi.org/10.1016/j.jenvman.2016.09.088> (2017).
62. Rahimi, F. *et al.* Pyrite nanoparticles derived from mine waste as efficient catalyst for the activation of persulfates for degradation of tetracycline. *J. Water Process Eng.* **40**, 101808. <https://doi.org/10.1016/j.jwpe.2020.101808> (2021).
63. Abinaya, M. *et al.* Reduction of hexavalent chromium and degradation of tetracycline using a novel indium-doped Mn₂O₃ nanorod photocatalyst. *J. Hazard. Mater.* **397**, 122885 (2020).
64. Roy, N., Alex, S. A., Chandrasekaran, N., Mukherjee, A. & Kannabiran, K. A comprehensive update on antibiotics as an emerging water pollutant and their removal using nano-structured photocatalysts. *J. Environ. Chem. Eng.* **9**, 104796. <https://doi.org/10.1016/j.jece.2020.104796> (2021).
65. Galedari, M., Ghazi, M. M. & Mirmasoomi, S. R. Photocatalytic process for the tetracycline removal under visible light: Presenting a degradation model and optimization using response surface methodology (RSM). *Chem. Eng. Res. Des.* **145**, 323–333 (2019).
66. Eskandarian, M. R., Choi, H., Fazli, M. & Rasoulifard, M. H. Effect of UV-LED wavelengths on direct photolytic and TiO₂ photocatalytic degradation of emerging contaminants in water. *Chem. Eng. J.* **300**, 414–422. <https://doi.org/10.1016/j.cej.2016.05.049> (2016).
67. Dong, D. *et al.* Photocatalytic degradation of phenanthrene and pyrene on soil surfaces in the presence of nanometer rutile TiO₂ under UV-irradiation. *Chem. Eng. J.* **158**, 378–383 (2010).
68. Ke, Y. *et al.* Sulfidation behavior and mechanism of zinc silicate roasted with pyrite. *Appl. Surf. Sci.* **435**, 1011–1019 (2018).
69. Wang, L. *et al.* S-scheme heterojunction photocatalysts for CO₂ reduction. *Matter* **5**, 4187–4211 (2022).
70. Park, H. *et al.* CoS@TiO₂ S-scheme heterojunction photocatalyst for hydrogen production from photoinduced water splitting. *J. Clean. Prod.* **319**, 128819 (2021).
71. Wang, Y. *et al.* Engineering hierarchical FeS₂/TiO₂ nanotubes on Ti mesh as a tailorable flow-through catalyst belt for all-day-active degradation of organic pollutants and pathogens. *J. Hazard. Mater.* **438**, 129501 (2022).
72. Kantar, C., Oral, O., Urken, O. & Oz, N. A. Role of complexing agents on oxidative degradation of chlorophenolic compounds by pyrite-Fenton process: Batch and column experiments. *J. Hazard. Mater.* **373**, 160–167 (2019).
73. Lee, G. & Kang, M. Physicochemical properties of core/shell structured pyrite FeS₂/anatase TiO₂ composites and their photocatalytic hydrogen production performances. *Curr. Appl. Phys.* **13**, 1482–1489 (2013).
74. Rashid, J. *et al.* Stabilized fabrication of anatase-TiO₂/FeS₂ (pyrite) semiconductor composite nanocrystals for enhanced solar light-mediated photocatalytic degradation of methylene blue. *RSC Adv.* **8**, 11935–11945 (2018).
75. Pan, Y. *et al.* Fabrication of MIL-Fe (53)/modified g-C₃N₄ photocatalyst synergy H₂O₂ for degradation of tetracycline. *Separ. Purif. Technol.* **279**, 119661 (2021).
76. Yang, R. *et al.* One-step preparation (3D/2D/2D) BiVO₄/FeVO₄@rGO heterojunction composite photocatalyst for the removal of tetracycline and hexavalent chromium ions in water. *Chem. Eng. J.* **390**, 124522. <https://doi.org/10.1016/j.cej.2020.124522> (2020).
77. Yu, H. *et al.* Enhanced photocatalytic degradation of tetracycline under visible light by using a ternary photocatalyst of Ag₃PO₄/AgBr/g-C₃N₄ with dual Z-scheme heterojunction. *Separ. Purif. Technol.* **237**, 116365. <https://doi.org/10.1016/j.seppur.2019.116365> (2020).
78. Guo, F., Huang, X., Chen, Z., Sun, H. & Shi, W. Investigation of visible-light-driven photocatalytic tetracycline degradation via carbon dots modified porous ZnSnO₃ cubes: Mechanism and degradation pathway. *Separ. Purif. Technol.* **253**, 117518 (2020).
79. Kakavandi, B., Bahari, N., Kalantary, R. R. & Fard, E. D. Enhanced sono-photocatalysis of tetracycline antibiotic using TiO₂ decorated on magnetic activated carbon (MAC@T) coupled with US and UV: A new hybrid system. *Ultrason. Sonochem.* **55**, 75–85 (2019).
80. Zhu, X.-D., Wang, Y.-J., Sun, R.-J. & Zhou, D.-M. Photocatalytic degradation of tetracycline in aqueous solution by nanosized TiO₂. *Chemosphere* **92**, 925–932 (2013).
81. Khataee, A., Soltani, R. D. C., Karimi, A. & Joo, S. W. Sonocatalytic degradation of a textile dye over Gd-doped ZnO nanoparticles synthesized through sonochemical process. *Ultrason. Sonochem.* **23**, 219–230 (2015).
82. Yun, E.-T. *et al.* Visible-light-induced activation of periodate that mimics dye-sensitization of TiO₂: Simultaneous decolorization of dyes and production of oxidizing radicals. *Appl. Catal. B Environ.* **203**, 475–484 (2017).
83. Moradi, M. *et al.* Visible-light-driven photocatalytic inactivation of Escherichia coli by titanium dioxide anchored on natural pyrite. *Inorg. Chem. Commun.* **144**, 109913 (2022).
84. Takdastan, A., Kakavandi, B., Azizi, M. & Golshan, M. Efficient activation of peroxymonosulfate by using ferrous oxide supported on carbon/UV/US system: A new approach into catalytic degradation of bisphenol A. *Chem. Eng. J.* **331**, 729–743 (2018).
85. Jorfi, S., Kakavandi, B., Motlagh, H. R., Ahmadi, M. & Jaafarzadeh, N. A novel combination of oxidative degradation for benzotriazole removal using TiO₂ loaded on FeIIFe₂III₄@C as an efficient activator of peroxymonosulfate. *Appl. Catal. B Environ.* **219**, 216–230 (2017).
86. Rezaei, S. S. *et al.* Photocatalytic oxidation of tetracycline by magnetic carbon-supported TiO₂ nanoparticles catalyzed peroxydisulfate: Performance, synergy and reaction mechanism studies. *Separ. Purif. Technol.* **258**, 117936 (2021).
87. Linting, H., Kun, C., Huaping, D., Jianfa, L. & Yimin, L. Enhanced effect of pyrite on the removal of metronidazole by zero valent iron. *J. Colloid Interface Sci.* **600**, 775–783. <https://doi.org/10.1016/j.jcis.2021.05.093> (2021).
88. Amiri, R. *et al.* Carbon quantum dots decorated Ag/CuFe₂O₄ for persulfate-assisted visible light photocatalytic degradation of tetracycline: A comparative study. *J. Water Process Eng.* **47**, 102742 (2022).
89. He, X., Kai, T. & Ding, P. Heterojunction photocatalysts for degradation of the tetracycline antibiotic: A review. *Environ. Chem. Lett.* **19**, 4563–4601 (2021).
90. Gan, W. *et al.* Ag nanoparticles decorated 2D/2D TiO₂/g-C₃N₄ heterojunction for efficient removal of tetracycline hydrochloride: Synthesis, degradation pathways, and mechanism. *Appl. Surf. Sci.* **606**, 154837 (2022).
91. Yu, X. *et al.* Efficient visible light photocatalytic antibiotic elimination performance induced by nanostructured Ag/AgCl@Ti₃+TiO₂ mesocrystals. *Chem. Eng. J.* **403**, 126359. <https://doi.org/10.1016/j.cej.2020.126359> (2021).
92. Ren, L. *et al.* Defects-engineering of magnetic γ-Fe₂O₃ ultrathin nanosheets/mesoporous black TiO₂ hollow sphere heterojunctions for efficient charge separation and the solar-driven photocatalytic mechanism of tetracycline degradation. *Appl. Catal. B Environ.* **240**, 319–328. <https://doi.org/10.1016/j.apcatb.2018.08.033> (2019).
93. Li, C. *et al.* Fabrication of ternary Ag/La-black TiO₂-x photocatalyst with enhanced visible-light photocatalytic activity for tetracycline degradation. *J. Alloys Compd.* **891**, 161960. <https://doi.org/10.1016/j.jallcom.2021.161960> (2022).
94. Wu, S., Li, X., Tian, Y., Lin, Y. & Hu, Y. H. Excellent photocatalytic degradation of tetracycline over black anatase-TiO₂ under visible light. *Chem. Eng. J.* **406**, 126747. <https://doi.org/10.1016/j.cej.2020.126747> (2021).
95. Huang, Z. & Liu, H. Insights into the pathways, intermediates, influence factors and toxicological properties in the degradation of tetracycline by TiO₂-based photocatalysts. *J. Environ. Chem. Eng.* <https://doi.org/10.1016/j.jwatres.2018.07.025> (2023).
96. Wang, H. *et al.* Visible-light-driven removal of tetracycline antibiotics and reclamation of hydrogen energy from natural water matrices and wastewater by polymeric carbon nitride foam. *Water Res.* **144**, 215–225 (2018).
97. Han, C.-H. *et al.* Oxidation of tetracycline and oxytetracycline for the photo-Fenton process: Their transformation products and toxicity assessment. *Water Res.* **172**, 115514. <https://doi.org/10.1016/j.watres.2020.115514> (2020).

Acknowledgements

The authors gratefully acknowledge the financial support provided by the Iran University of Medical Sciences (IUMS) under Grant Number 98-4-99-16763.

Author contributions

M.H.F.: Data curation, Resources, Writing – original draft. A.N.: Data curation, Resources, Investigation. M.M.: Review & editing, Visualization. R.R.K.: Resources, Conceptualization, Writing – review & editing, Project administration, Funding acquisition, Supervision.

Competing interests

The authors declare no competing interests.

Additional information

Correspondence and requests for materials should be addressed to R.R.K.

Reprints and permissions information is available at www.nature.com/reprints.

Publisher's note Springer Nature remains neutral with regard to jurisdictional claims in published maps and institutional affiliations.



Open Access This article is licensed under a Creative Commons Attribution 4.0 International License, which permits use, sharing, adaptation, distribution and reproduction in any medium or format, as long as you give appropriate credit to the original author(s) and the source, provide a link to the Creative Commons licence, and indicate if changes were made. The images or other third party material in this article are included in the article's Creative Commons licence, unless indicated otherwise in a credit line to the material. If material is not included in the article's Creative Commons licence and your intended use is not permitted by statutory regulation or exceeds the permitted use, you will need to obtain permission directly from the copyright holder. To view a copy of this licence, visit <http://creativecommons.org/licenses/by/4.0/>.

© The Author(s) 2024